Structural Decay and Swelling Behavior of Soft Rocks: Experimental Insights and Constitutive Modeling

Shintaro Murao[1], Mamoru Kikumoto[1], Atsumi Isogai[2] and Kiyoshi Kishida[1]

1 Kyoto University, Kyoto, Japan

2 Japan Railway Construction, Transport and Technology Agency, Yokohama, Japan

Abstract: In mountain tunnels constructed in soft rocks with swelling or squeezing characteristics, deformation behaviors such as cracking or buckling of support structures are often reported during construction or after the tunnels are put into service. The behavior of soft rock generally depends on the contact area between mineral particles and the tensile strength of interparticle cementation, collectively referred to as the rock's structure. However, in soft rocks with swelling and squeezing characteristics, structural decay and recovery are influenced by mechanical and hydro-mechanical processes, which are believed to result in significant deformation. This study conducted slaking tests on mudstone, during which seismic wave velocities were measured, and X-ray CT imaging was performed. These experiments revealed structural decay during the slaking process. Swelling tests were also conducted, and the swelling behavior of the soft rock was examined. Furthermore, a constitutive model for soft rocks, incorporating structural decay within the framework of extended critical state theory, was proposed, and numerical simulations of the swelling tests were performed using this model.

Keywords: Azores Islands; Volcanic Rocks; Soft Rocks; VRS Empirical System.

1. Introduction

After the completion of mountain tunnels, deformation or buckling of steel supports, cracking and spalling of lining concrete, and floor heaving are often observed either immediately or after a certain period (Kobayashi, 2020). When such deformations occur after the tunnel has been put into service, countermeasures are required, which may involve a reassessment of the support structure, removal work, and reconstruction. These measures can incur significantly higher costs compared to those taken during construction.

The primary causes of post-construction deformations are considered to be:

1. Insufficient evaluation of the mechanical properties of the surrounding ground.
2. Ingress of water into the ground around the tunnel, leading to long-term swelling behavior, which results in strength degradation and softening of the rock.

In this study, a series of wet-dry cycle tests was conducted using tuffaceous mudstone samples collected from a tunnel construction site. Simultaneously, elastic wave velocity measurements were performed to observe the deterioration behavior of the rock under repeated wet-dry conditions. Furthermore, tunnel excavation analyses were carried out using two different models: the Modified Cam-Clay model and a swelling-considered Modified Cam-Clay model. The impact of swelling on tunnel deformation was then evaluated. This paper presents the findings of these investigations, building upon the work of Murao et al. (2025) with additional experimental data.

2. Laboratory Tests

Laboratory tests were conducted using mudstone specimens collected from a tunnel construction site where deformation was reported. The tests included a slaking test, elastic wave velocity measurements, and CT imaging.

2.1 Slaking Test

A slaking test was performed to investigate the degradation characteristics of the mudstone under wet-dry cycles. The block specimen was immersed in distilled water, and the progress of slaking was visually observed and recorded through photographs.

Photo 1 shows the state of the specimen after immersion. The specimen began to crumble immediately upon contact with water, and after one hour, it had completely disintegrated into fine particles, losing its original shape. However, no further disintegration into a slurry was observed even after 24 hours.

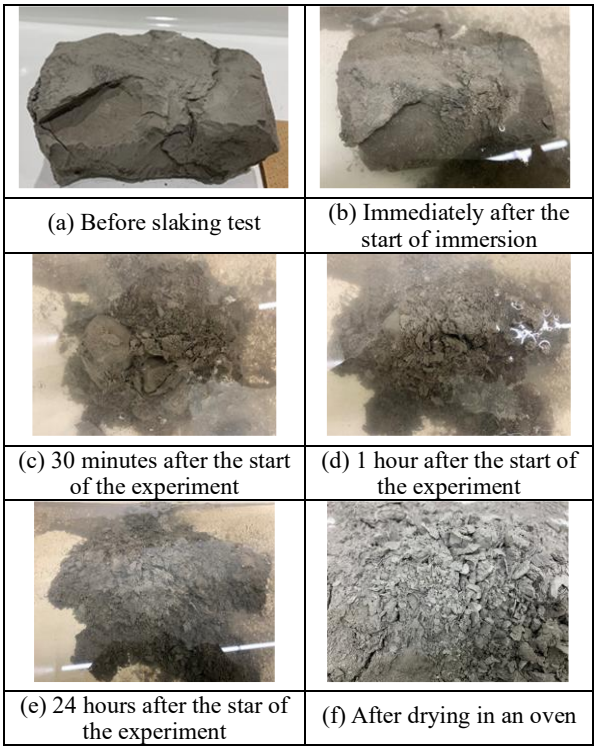

(a) Before slaking test | (b) Immediately after the start of immersion

(c) 30 minutes after the start of the experiment | (d) 1 hour after the start of the experiment

(e) 24 hours after the star of the experiment | (f) After drying in an oven

Photo 1 Slaking process

Based on the slaking classification chart (Japanese Geotechnical Society, 2020a), the specimen was visually assessed and assigned a slaking index of 3. The absence of swelling and slurry formation suggests a collapse-type degradation, likely indicative of a mudstone containing a high proportion of Ca-type smectite.

2.2 Elastic Wave Velocity Measurement

Three cylindrical specimens (Test-piece-1 to 3) with a diameter of 5 cm and a height of 10 cm were prepared from the mudstone for elastic wave velocity measurements. To evaluate the progression of rock degradation under wet-dry cycles, wave velocities were measured at the end of each drying and wetting phase.

During the drying phase, the specimens were placed in a constant-temperature drying oven at 40°C for approximately 20 days. For the wetting phase, they were placed in a sealed plastic box filled with ion-exchanged water to maintain a humidity of 100% for about 40 days. This wet-dry cycle was repeated, and both the mass and elastic wave velocities of the specimens were measured at the end of each phase.

The pulse transmission method specified by the Japanese Geotechnical Society (2020b) was used to measure the wave velocities. After the wetting phase, the specimens had a moisture content of approximately 4%.

The results in Figs. 1 and 2 show that both P-wave and S-wave velocities decreased after the wetting phases compared to the drying phases. Specifically, the P-wave velocity decreased by approximately 0.8 km/s, and the S-wave velocity decreased by approximately 0.1 km/s. This reduction in velocity is attributed to water infiltration into the rock's internal pores, reducing the effective stiffness of the material.

Furthermore, as the number of wet-dry cycles increased, both P-wave and S-wave velocities exhibited a gradual decline. This suggests that repeated cycles caused an increase in porosity and microcrack development, leading to further degradation of the rock.

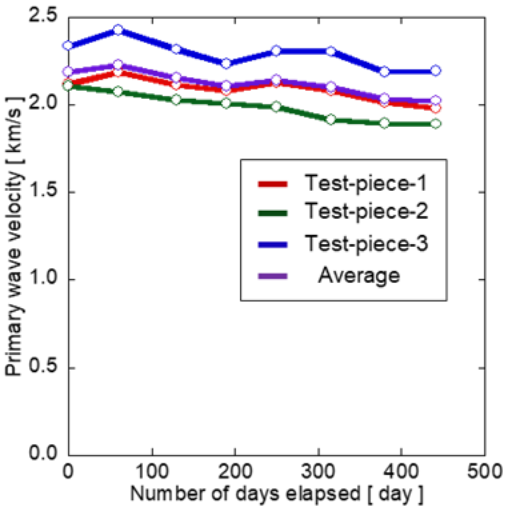

(a) After each dry process

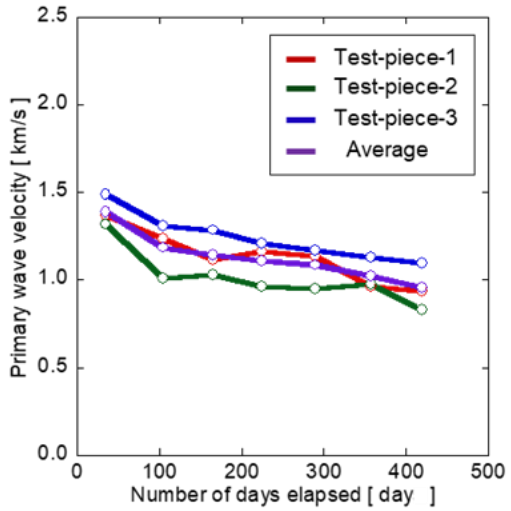

(b) After each wet process

Fig. 1 Time-related changes of P-wave velocity

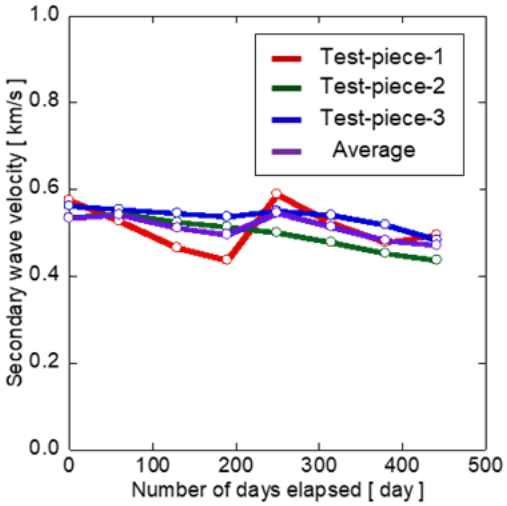

(a) After each dry process

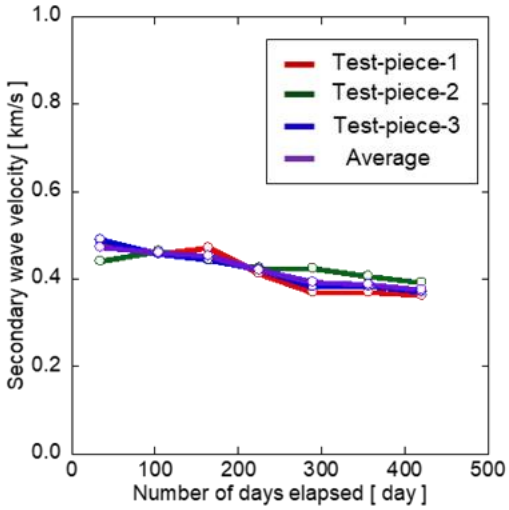

(b) After each wet process

Fig. 2 Time-related changes of P-wave velocity

2.3 CT Imaging

CT imaging was performed before and after the eight cycles of wet-dry testing to observe the internal structural changes of the specimens. Images were taken after the drying process, with the specimens having undergone 20 days of drying at 40°C.

To enhance image clarity, beam hardening effects were removed, and the average CT values were calculated for normalization. While this adjustment improved the visibility of the internal structure, care was taken when comparing brightness levels across images due to potential differences in average CT values.

Fig. 3 present the CT images taken before and after the wet-dry cycles, respectively. In **Fig. 3**(a), (c), (e), the initial images show minor pre-existing cracks and pores within the specimen. However, after the cycles, as shown in **Fig. 3**(b), (d), (f), notable crack propagation and the formation of new cracks were observed.

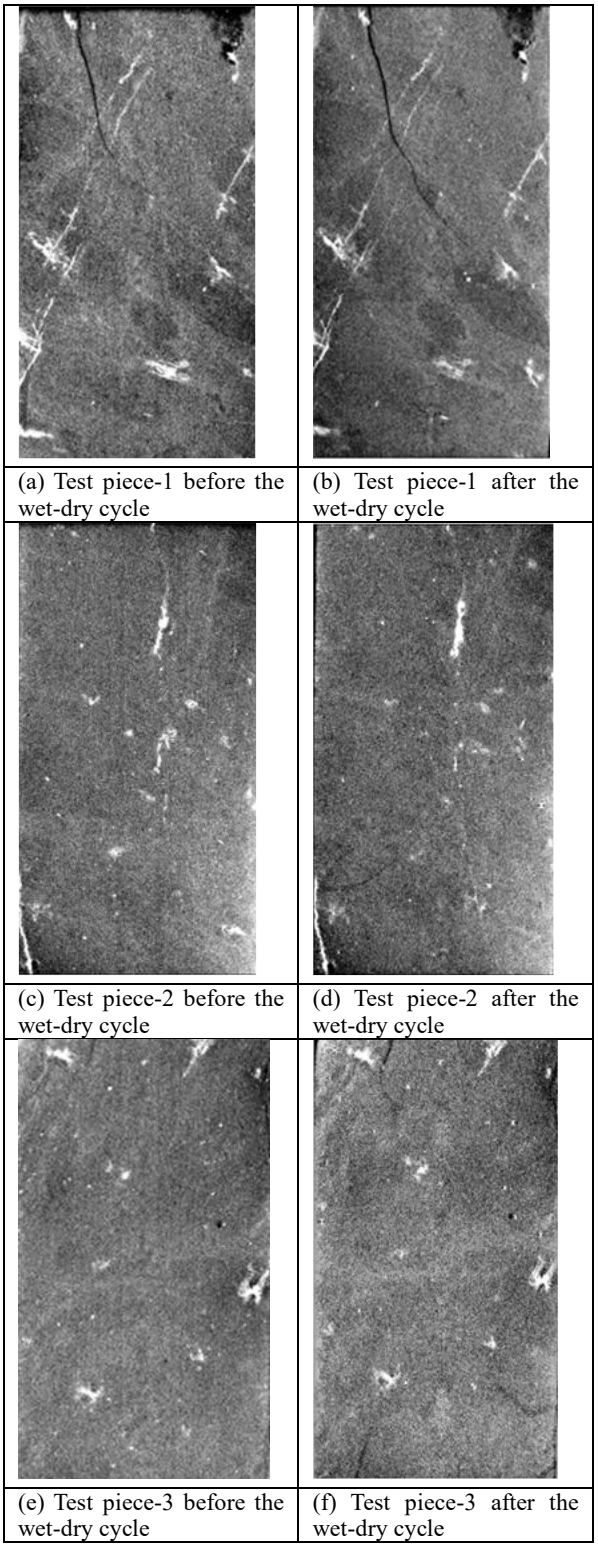

(a) Test piece-1 before the wet-dry cycle | (b) Test piece-1 after the wet-dry cycle

(c) Test piece-2 before the wet-dry cycle | (d) Test piece-2 after the wet-dry cycle

(e) Test piece-3 before the wet-dry cycle | (f) Test piece-3 after the wet-dry cycle

Fig. 2 Location and geotectonic framework of the Azores Archipelago (Santos et al., 2024).

The cracks predominantly expanded from the specimen's ends and along pre-existing weak planes. This is likely due to water infiltration during the wetting phases, which caused localized swelling. The differential pressure between the expanded

regions and the surrounding material may have contributed to crack initiation and propagation.

These results suggest that the degradation process was accelerated by repeated wet-dry cycling, leading to progressive internal damage. Understanding the relationship between microstructural changes and mechanical property degradation will provide further insights into the behavior of mudstone under similar environmental conditions.

3. Application of a Swelling Model to a Constitutive Equation Based on Critical State Theory and Finite Element Analysis

3.1 Constitutive Model

Yuan (2024), based on the ideas of Xie et al. (2007) and Liu et al. (2021), incorporated swelling volume into a constitutive model based on critical state theory (the Modified Cam Clay model) to account for the degradation of the mechanical properties of the ground. In this model, the softening caused by the progression of swelling behavior is represented by the shrinkage of the yield surface due to a decrease in consolidation yield stress.

The parameters used in this model are defined as follows: v is the specific volume, e is the void ratio, λ is the compression index, κ is the swelling index, p is the consolidation stress, p_r is the reference stress, v_r is the reference specific volume on the normal consolidation line, and $v_{\kappa 0}$ is the specific volume at the reference stress p_r on the initial swelling line. These variables are set as follows, and the consolidation curve in the v - ln$p$ relationship is shown in **Fig. 3**.

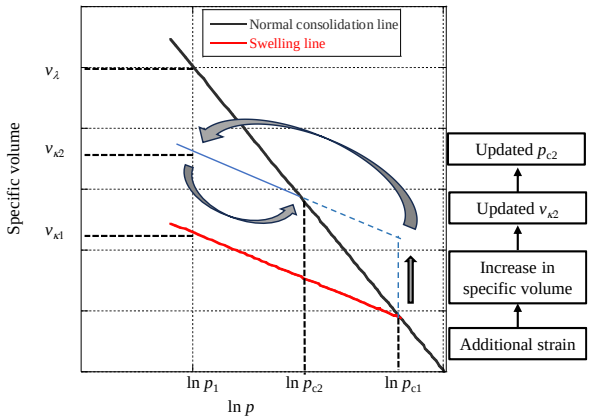

Fig. 3. Update of the swelling line and reduction in consolidation yield stress in the e-ln p plane of the swelling MCC model (Yuan, 2024).

$$v = 1 + e \tag{1}$$

$$v = v_r - \lambda \ln\left(\frac{p}{p_r}\right) \tag{2}$$

$$v = v_{\kappa 0} - \kappa \ln\left(\frac{p}{p_r}\right) \tag{3}$$

Here, the initial consolidation yield stress p_{c0} is defined as the consolidation stress at the intersection of the normal consolidation line and the initial swelling line. Based on this, the normal consolidation line and the swelling line are determined.

Next, the total strain (ε_{total}), shear strain (ε_{shear}), and volumetric strain (ε_{volume}) satisfy the following relationships:

$$\varepsilon_{total} = \varepsilon_{shear} + \varepsilon_{volume} \tag{4}$$

Furthermore, the swelling strain ($\varepsilon_{swelling}$) is added as an increment of volumetric strain in Equation (4) under plastic conditions. In the normal consolidation state, the swelling strain is set to zero. Given this, if v_0 is the specific volume, v, on the initial swelling line, the increment of volumetric strain is defined as follows for the swelling state and the normal consolidation state:

$$\Delta\varepsilon_{volume} = \begin{cases} \varepsilon_{swelling} & \left(v < v_r - \lambda \ln\left(\frac{p}{p_r}\right)\right) \\ 0 & \left(v = v_r - \lambda \ln\left(\frac{p}{p_r}\right)\right) \end{cases} \tag{5}$$

$$v = v_0\left(1 + \varepsilon_{volume}\right) \tag{6}$$

From Equation (6), the specific volume, v, increases, and from Equation (7), the swelling line, v_κ, is updated.

$$v_\kappa = v + \kappa \ln\left(\frac{p}{p_r}\right) \tag{7}$$

As the swelling line is updated and the specific volume, v_κ, increases, the normal consolidation stress, p_c, is updated according to Equation (8), as shown in **Fig. 3**.

$$p_c = p_r \exp\left(\frac{v_r - v_\kappa}{\lambda - \kappa}\right) \tag{8}$$

From the above, the yield surface defined in the MCC model is expressed as:

$$f = q^2 - M^2[p'(p_c - p')] \tag{9}$$

Taking this into account, the swelling strain, $\varepsilon_{swelling}$, generated in the plastic state is added to the volumetric strain, ε_{volume}, resulting in a decrease in the normal consolidation stress, p_c, and a contraction of the yield surface, as shown in **Fig. 4**. This contraction of the yield surface represents the softening of the ground due to swelling behavior.

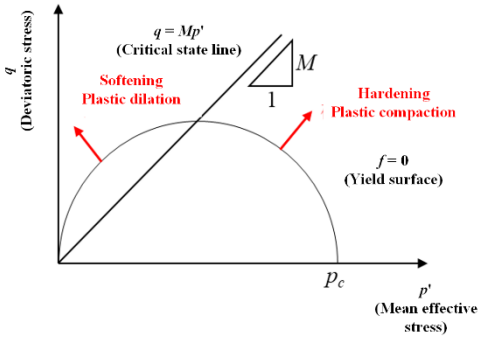

Fig. 4. Yield surface and critical state line

3.2 Simulation for triaxial test

A numerical element analysis was conducted using the analysis model shown in **Fig. 5**, employing both the MCC model and the swelling MCC model to simulate a drained triaxial compression test.

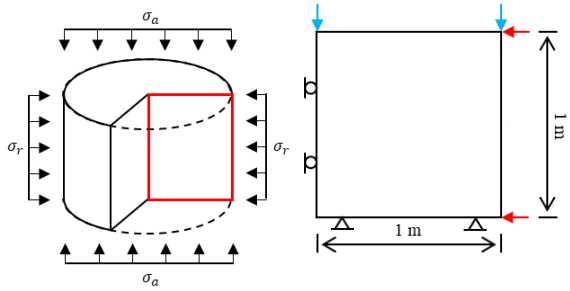

(a) Triaxial test (b) Simulation model

Fig. 5. Simulation model for triaxial test.

For the analysis, an axisymmetric model was used with an element of 1 m × 1 m. The model was subjected to lateral confining pressure and an axial strain rate at the top, and displacement-controlled loading was applied up to an axial strain of 15%. The parameters used in the analysis are listed in **Table 1**. These physical properties were determined primarily based on laboratory tests conducted on field samples.

Table 1 Input parameters

Dry density [kg/m^3]	1956
Wet density [kg/m^3]	2124
Compression index [-]	0.011
Swelling index [-]	0.115
Critical state stress ratio [-]	1.093
Reference pressure [kPa]	100
Poisson's ratio [-]	0.30
Hydraulic conductivity [m/s]	4.31×10^{-8}

3.3 Simulation results

This section discusses the element analysis of drained triaxial compression tests using the MCC model and the swelling MCC model. Each simulation started in an isotropic consolidation state with a confining pressure of 1000 kPa. Then, an axial strain rate of 5.0×10^{-6} per step was applied from the top of the analysis model, and loading continued until the axial strain reached 15% (**Table 2**). The strain rate here refers to the amount of strain applied per step.

Table 2 Procedure of Element Analysis for Drained Triaxial Compression Test (MCC Model)

(1) Apply an axial strain rate of 5.0×10^{-4} [%/step] for 20 steps
(2) Set the strain rate to 0 and hold for 220 steps.
(3) Repeat steps (1) - (2) for 1500 cycles.

For the swelling MCC model, an additional phase was introduced in which a swelling strain rate of 3.3×10^{-8} per step was applied, and the simulation was conducted under these conditions (**Table 3**).

Table 3 Procedure of Element Analysis for Drained Triaxial Compression Test (MCC Model with swelling)

(1) Apply an axial strain rate of 5.0×10^{-4} [%/step] for 20 steps.
(2) Set the strain rate to 0 and hold for 20 steps.
(3) Apply a swelling strain rate of 3.3×10^{-5} [%/step] for 100 steps.
(4) Set the strain rate to 0 and hold for 100 steps.
(5) Repeat steps (1) – (4) for 1500 cycles.

In **Fig. 6**, the red line represents the effective stress path, the black line represents the critical state line, the blue line represents the initial yield surface, and the green line represents the yield surface at the end of the test.

For both models, the confining pressure was initially applied isotropically, and as the axial strain increased, the deviatoric stress also increased. In the MCC model, the critical state was maintained after reaching the critical state line, and ultimately, the yield surface expanded, representing hardening behavior during the triaxial compression test.

In contrast, the MCC model with swelling initially exhibited a similar behavior to the MCC model until the effective stress path reached the critical state line. However, after reaching the critical state line, the path extended to the left of the critical state line.

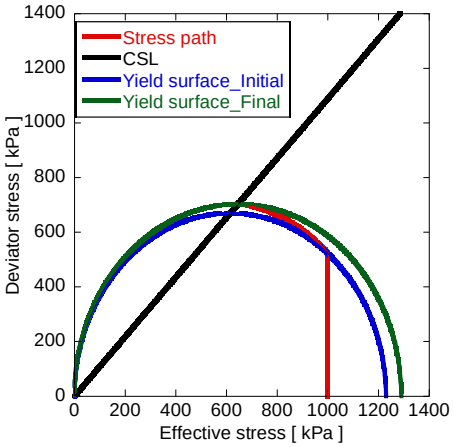

(a) Modified Cam Clay model

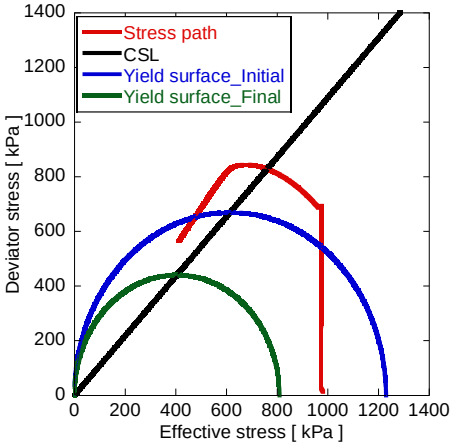

(b) Modified Cam Clay model with swelling

Fig.6 Effective stress path through the triaxial test simulation.

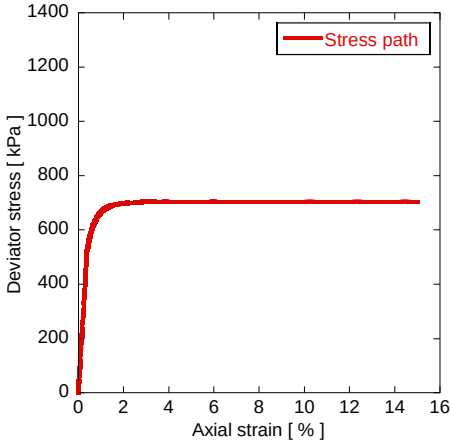

(a) Modified Cam Clay model

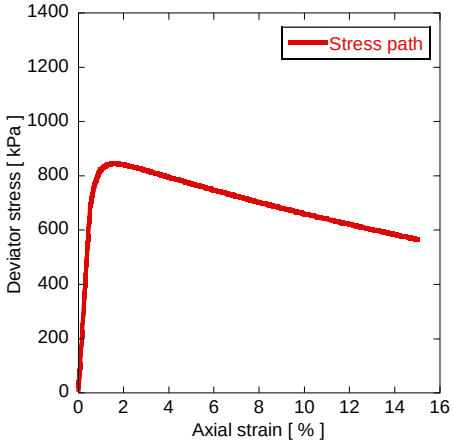

(b) Modified Cam Clay model with swelling

Fig.7 Relationship between deviatoric stress and axial strain in the triaxial test simulation.

From the axial strain–deviatoric **stress** relationship (**Fig. 7**), it is observed that the deviatoric stress decreases after reaching its peak. Additionally, the axial strain–volumetric strain relationship (**Fig. 8**) shows that the volumetric strain increases in the compression direction more gradually compared to the MCC model. These two points indicate that the model captures plastic expansion behavior after reaching the critical state, which represents softening behavior during the triaxial compression test.

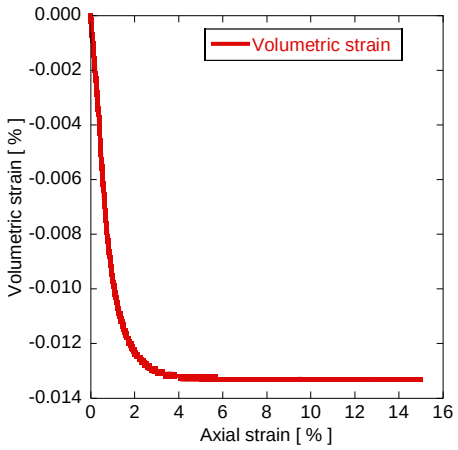

(a) Modified Cam Clay model

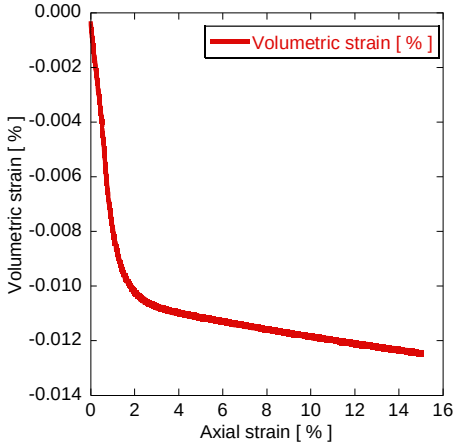

(b) Modified Cam Clay model with swelling

Fig.8 Relationship between volumetric strain and axial strain in the triaxial test simulation.

4. Concluding Remarks

In this study, physical property tests were conducted using a swelling-prone material, and it was confirmed that both elastic wave velocity and elastic modulus decreased with repeated drying and wetting cycles. Additionally, CT images visualized an increase in the number of cracks over time.

Furthermore, a constitutive model incorporating swelling characteristics proposed by Yuan (2024) was employed to perform undrained triaxial compression simulations. The analysis incorporating swelling characteristics confirmed that the deviatoric stress decreased over time.

References

Japanese Geotechnical Society (2020a): *JAPANESE GEOTECHNICAL SOCIETY STANDARDS Laboratory Testing Standards of Geomaterials* (Vol.1), JGS 2124 Method for rock slaking test.

Japanese Geotechnical Society (2020b): *JAPANESE GEOTECHNICAL SOCIETY STANDARDS Laboratory Testing Standards of Geomaterials* (Vol.1), JGS 2564 Method for laboratory measurement of ultrasonic wave velocity of rock by pulse test.

Kobayashi, H. (2020): *Study on the inhibitory effect of a novel tunnel invert structure for preventing floor heaving after completion of a mountain tunnel*, Ph. D thesis at Kyoto University. (in Japanese) https://doi.org/10.14989/doctor.r13359

Liu, X., Yamada, S., Kyoya, T. (2021): Stability evaluation analysis of tunnels applying a constitutive law which considering softening deterioration phenomena of rock mass due to swelling, 15th Japan Symposium on Rock Mechanics, pp. 97-102. (In Japanese)

Murao, S., Kikumoto, M., Isogai, A., Kishida, K.: A study on the influence of swelling of the ground on the deformation of tunnels, Proceedings of the 16th Japan Symposium on Rock Mechanics, 36 – 41, 2025. (in Japanese).

Xie, M., Wang, W. De Jonge, J. & Kolditz, O. (2007): Numerical Modelling of Swelling Pressure in Unsaturated Expansive Elasto-Plastic Porous Media, Transport in Porous Media, 66, 311-339. https://doi-org.kyoto-u.idm.oclc.org/10.1007/s11242-006-0013-0

Yuan, K. (2024): *Mechanism investigation on weathered mudstone slope deformation under excavation process with geological complexity and folded structure*, Ph. D Thesis at Kyoto University. https://doi.org/10.14989/doctor.k25262